Journal of ELECTRONIC MATERIALS, Vol. 45, No. 12, 2016
DOI: 10.1007/s11664-016-4892-8

Effect of Silicon Carbide Nanoparticles on the Grain Boundary Segregation and Thermoelectric Properties of Bismuth Doped $Mg_2Si_{0.7}Ge_{0.3}$

NADER FARAHI,[1] SAGAR PRABHUDEV,[2] MATTHIEU BUGNET,[2] GIANLUIGI A. BOTTON,[2] JAMES R. SALVADOR,[3] and HOLGER KLEINKE[1,4]

1.—Department of Chemistry and Waterloo Institute for Nanotechnology, University of Waterloo, Waterloo, ON N2L 3G1, Canada. 2.—Materials Science and Engineering Department, McMaster University, Hamilton, ON L8S 4L8, Canada. 3.—General Motors Research and Development Center, Warren, MI 48154, USA. 4.—e-mail: kleinke@uwaterloo.ca

The effect of silicon carbide (SiC) nanoparticles on the thermoelectric properties of $Mg_2Si_{0.676}Ge_{0.3}Bi_{0.024}$ was investigated. Increasing the concentration of SiC nanoparticles systematically reduces the electrical conductivity from 431 Ω^{-1} cm^{-1} for the pristine sample to 370 Ω^{-1} cm^{-1} for the sample with 1.5 wt.% SiC at 773 K, while enhancing the Seebeck coefficient from -202 μV K^{-1} to -215 μV K^{-1} at 773 K. In spite of the high thermal conductivity of SiC, its additions could successfully decrease the lattice thermal conductivity from 3.2 W m^{-1} K^{-1} to 2.7 W m^{-1} K^{-1} at 323 K, presumably by adding more interfaces. The Z contrast transmission electron microscopy imaging (Z = atomic number) and energy dispersive x-ray spectroscopy revealed bismuth segregation at the grain boundary. In summary, the figure of merit reached its maximum value of 0.75 at 773 K for the sample containing 0.5 wt.% SiC.

Key words: Magnesium silicide, silicon carbide, thermoelectrics, nanocomposites

INTRODUCTION

After several decades of successfully supplying energy for space and terrestrial exploration missions from Voyager to Curiosity,[1,2] thermoelectric (TE) materials are now on the verge of commercialization for waste heat recovery for both stationary applications, passenger, and heavy duty vehicles.[3] In order to reduce both fossil fuel consumption and CO_2 emission, it is important to recover as much waste heat as possible. However, certain criteria need to be fulfilled for implementing TE materials in large scale industrial applications. The ideal materials for this purpose should not only maintain high efficiency to enhance fuel energy utilization, but also should be made of cost effective, naturally abundant and non-toxic elements. The thermoelectric figure of merit, zT, has been used as a norm to measure the efficiency of the material; zT is defined via $zT = TS^2\sigma\,\kappa^{-1}$, where T, S, κ, and σ represent absolute temperature, Seebeck coefficient, thermal conductivity, and electrical conductivity, respectively.[4]

Magnesium silicide based TE materials are projected to be cost effective and environmentally benign next generation TE materials.[5] Mg_2Si crystallizes in the high symmetry space group $Fm\bar{3}m$ and has a fairly large band gap of 0.77 eV.[6] It exhibits high thermal conductivity and low electrical conductivity, resulting in a low zT of around 0.12 at 850 K.[7] This can be improved by alloying and doping, both typically done on the Si site. Substituting around 30 at.% Ge for Si dramatically reduces the room temperature thermal conductivity from 10 W m^{-1} K^{-1} to below 3 W m^{-1} K^{-1}, yielding a maximum figure of merit zT = 0.7 at 773 K in the

(Received May 20, 2016; accepted August 18, 2016; published online September 1, 2016)

case of $Mg_2Si_{0.677}Ge_{0.3}Bi_{0.023}$.[8] Doping with Bi increases the electrical conductivity by nominally adding one electron for each substituted Si atom to the material. Since Bi^{3-} is larger than Si^{4-}, enlarging the unit cell through Ge solid solution could potentially increase the solubility of Bi.[9] A third way to further enhance the thermoelectric properties is through nano-inclusions.[10] Embedding a suitable nanoparticle could improve the thermopower by filtering low energy electrons and maintaining electrical conductivity while mitigating thermal conductivity through scattering of mid- to long-wavelength phonons.[11,12] So far TiO_2[13] Si nanoparticles[14] and single-wall carbon-nanohorns (SWCNH)[15] were studied as nano-inclusions in Mg_2Si materials, but were not as effective as alloying Mg_2Si with tin[16] or germanium[8] in reducing the thermal conductivity.

Although bulk SiC has high room temperature thermal conductivity,[17] adding small amounts of SiC nanoparticles reduced the thermal conductivity of $Bi_{0.5}Sb_{1.5}Te_3$, $Bi_2Te_{2.7}Se_{0.3}$[18] and Bi_2Te_3 materials.[19] With this contribution we discuss the effect of SiC nanoparticles on the thermoelectric properties of $Mg_2Si_{0.7}Ge_{0.3}$ based materials. To the best of the authors' knowledge, no previous studies of SiC nanocomposites with $Mg_2Si_{1-x}Ge_x$ solid solutions have been reported. In fact, studies investigating the effects of nanocomposites on $Mg_2Si_{1-x}Ge_x$ solid solutions are scarce. Our previous work investigating the effect of multi-wall carbon nanotube composites[20] has inspired the present investigation.

EXPERIMENTAL

$Mg_2Si_{0.676}Ge_{0.3}Bi_{0.024}$ samples were prepared by combining the elements according to the stoichiometric ratios in argon filled glove box. Mg chips (99.98%, Sigma Aldrich, 4–30 mesh), Si powder (99.9%, Alfa Aesar, −100 mesh), Ge pieces (99.9999+%, Alfa Aesar, ≤2 cm), and Bi granules (99.99%, Sigma Aldrich) were used for the synthesis. The detailed synthesis conditions were previously described.[8]

An Inel powder x-ray diffractometer with Cu-$K\alpha_1$ radiation and a position sensitive detector was used to determine the purity of the synthesized samples. Powder x-ray diffraction patterns (Figure S1, available in the Supplementary Information) revealed traces of MgO, which is a common side product in Mg_2Si based compounds.[21] The synthesized samples were ground into powders, manually mixed, and then divided into four batches. Varying amounts of silicon carbide (SiC) nanoparticles (Alfa Aesar, β modification, 45–55 nm) were added to each batch and mixed for 3–5 min using a Fisher Scientific vortex mixer until no SiC nanoparticle agglomerations were observed.

To consolidate the samples for physical property measurements, an Oxy-Gon hot press was used to press the mixtures in an Ar atmosphere at 973 K for 2 h under 56 MPa. To reduce strain and stress on the pellets, the pressure was released during cooling. The pressed pellets were 12.7 mm in diameter and 2 mm in thickness. Thermal diffusivity (α) of the pressed pellets was measured under Ar gas flow using the Anter Flashline FL3000 thermal properties analyzer between 300 K and 800 K. The obtained values were then multiplied by the density (d) of the pellets, as measured via the Archimedes method, and the specific heat (C_p) of the compounds, as calculated from the Dulong-Petit approximation, to obtain thermal conductivity (κ), $\kappa = \alpha\, d\, C_p$. The measured densities together with the calculated specific heat of all the samples are available in Table S1. The accuracy of Dulong-Petit approximation on the specific heat of the bismuth doped $Mg_2Si_{1-x}Ge_x$ system was confirmed in our previous study.[8] Since adding SiC nanoparticles only changed the calculated specific heat by $<1\%$, which is well within the error of the measurement of 5%, the values of the specific heat calculated from Dulong–Petit approximation were applied to obtain the thermal conductivity.

The electrical conductivity (σ) and Seebeck coefficient (S) were subsequently measured on rectangular bars with the dimensions of roughly 12 mm × 2 mm × 2 mm cut from the diffusivity specimen. The measurements were performed under helium atmosphere between 300 K and 800 K by using the ULVAC-RIKO ZEM-3 apparatus. Estimated experimental errors are 3% for the Seebeck coefficient, and 5% both for the electrical and thermal conductivity, which results in an error of about 10% for the figure of merit.[22]

Finally, using the same bars, we performed Hall effect measurements using a cryostat equipped with a 5 Tesla (T) magnet and with a Linear Research AC resistance bridge (AC = alternating current). These measurements were done from −3 T to 3 T and from 5 K to 300 K. The carrier concentration (n) was calculated from the Hall coefficient, R_H, using the relationship $n = R_H^{-1}e^{-1}$, where e is the fundamental charge, and assuming a Hall factor equal to 1.

To substantiate the existence and examine the dispersion of nanoparticles within the samples at the micron length scale, scanning electron microscopy (SEM) analysis was carried out on parts of the pellet with the largest SiC amount, i.e. 1.5 wt.%, (Figure S2) using a Zeiss ULTRA electron microscope associated with an energy dispersive x-ray (EDX) device, EDAX Pegasus 1200.

Elemental analyses were performed within grains and across grain boundaries using energy dispersive x-ray spectroscopy (XEDS) in a double corrected FEI-Titan cubed transmission electron microscope (TEM), operated at 300 kV in scanning transmission electron microscope (STEM) mode with high-angle annular dark-field imaging (HAADF) imaging (Z contrast). The Mg-K, Si-K, Ge-K, and Bi-L spectral lines were used. The sample with the best thermoelectric performance, i.e.

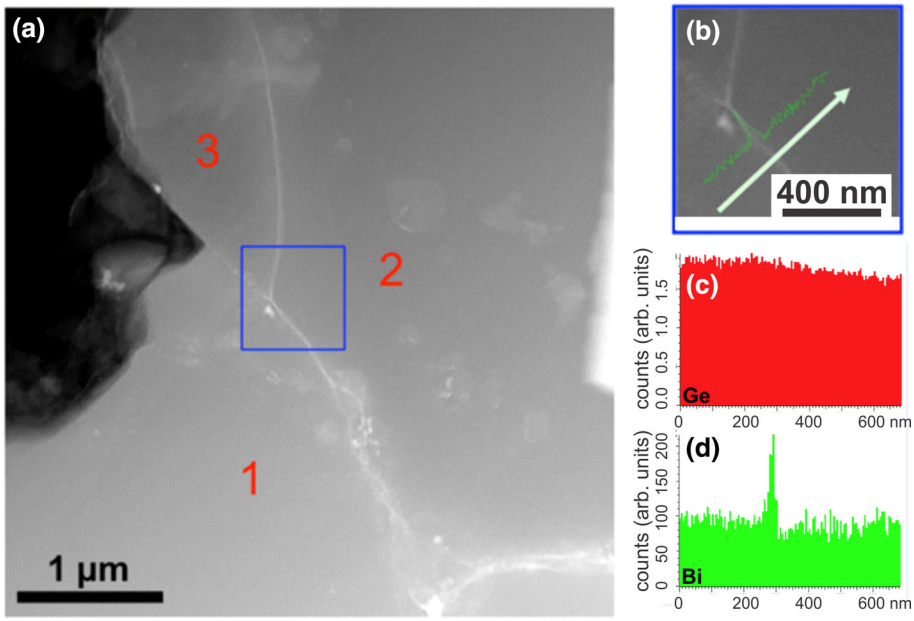

Fig. 1. (a) Low-magnification STEM-HAADF image with the magnified area of interest for the line scan; (b) elemental EDX line profile of Bi across the grain boundary; (c) Ge line profile along along the arrow shown in (b); (d) Bi line profile along along the arrow shown in (b).

0.5 wt.% SiC, was thinned down to electron transparency by the wedge-polishing technique using a multiprep apparatus (Allied Inc.), and further argon ion milled using a Gentle Mill (Technoord Linda Inc.).

RESULTS AND DISCUSSION

Low-magnification STEM imaging as shown in Fig. 1a revealed the polycrystalline nature of the $Mg_2Si_{0.676}Ge_{0.3}Bi_{0.024}$/0.5% SiC nanocomposite. The three grains selected for analyses are identified as 1, 2, and 3. In contrast to the bulk of the grain, grain boundaries exhibit brighter intensities, which could be related to the segregation of Ge and/or Bi. In order to confirm this hypothesis, alongside the STEM imaging discussed in Fig. 1, we carried out elemental analyses via EDX. As shown in Fig. 1b, elemental line scans for Ge and Bi were performed across the grain boundary. Figure 1b is representative of a number of boundaries investigated; the results indicate an accumulation of Bi along the grain boundary, but no clear Ge concentration changes. In contrast, it is worth mentioning that segregation of Ge was observed in multiwall carbon nanotubes (MWCNTs) samples,[20] which suggests the possibility of grain boundary engineering. Specifically, the type of nano-inclusion can be used to alter the chemical composition of the grain boundaries of the sample and thereby the thermoelectric properties of the material.

EDX spot analyses were carried out over a region within the three grains (1, 2, and 3) of Fig. 1a to examine the elemental distributions in the bulk of the grain. The quantified results (Table S2) confirm the presence of Ge and Bi in the bulk of the grain. Grain 1 seemed to be rich in Ge compared to the nominal Ge content; since Ge and Bi both compete to replace Si in the structure,[8] the excess amount of Ge found inside the grain is consistent with more Bi observed at the boundaries.

The electrical conductivity of all $Mg_2Si_{0.676}Ge_{0.3}Bi_{0.024}$/SiC nanocomposites is shown in Fig. 2. Adding SiC reduces the electrical conductivity monotonically from 545 Ω^{-1} cm^{-1} to 420 Ω^{-1} cm^{-1} at 325 K, i.e. by 23%. Such a consistent reduction was expected due to its insulating character, as well as the additional interfaces arising from introducing more SiC nanoparticles. The difference between the electrical conductivity of the samples becomes less significant at higher temperatures, e.g. 6% at 773 K (395 Ω^{-1} cm^{-1} compared to 370 Ω^{-1} cm^{-1}) for the samples containing 0.5 wt.% and 1.5 wt.% SiC, respectively. All samples containing SiC exhibit smaller reductions in high temperature electrical conductivity (85–88% of the value at 323 K) compared to the pristine sample reaching only 79% of its initial value at 323 K. This could be due to the existence of Bi at the grain boundaries of nanocomposites that can facilitate charge carrier transport. The opposite effect was seen in the case of MWCNT nanocomposites,[20] where the segregation of Ge at the boundaries led all the MWCNT containing samples to have around 93% of their initial values at 323 K with the matrix showing 105% of its 323 K value. The low temperature electrical conductivity of the composites obtained from the Hall measurements, shown in Figure S3, is in good agreement with our high temperature data.

Because of the low concentration of the inert nanoparticles in the sample, no significant changes were observed in the carrier concentration of the samples containing SiC (Fig. 3a), and all samples displayed a virtually temperature independent carrier concentration of around 6.5×10^{19} cm^{-3}. Therefore, the reduction in electrical conductivity must have come from lower mobility. The sample containing 1.5 wt.% SiC exhibits the lowest mobility among all samples with 37 cm^2 V^{-1} s^{-1} at 300 K, with the other ones having >42 cm^2 V^{-1} s^{-1} (Fig. 3b). The sample containing Si nanoparticles published by Kauzlarich et al. had a mobility of around 13 cm^2 V^{-1} s^{-1} at 300 K (Table I), which is approximately one third the value of our SiC nanocomposites. This could be due to its very high carrier concentration that increased the electron–phonon interaction. To better understand the effect of SiC nanoparticles on the mobility of charge carriers, considering the significance of acoustic phonon scattering the mean free path of carriers (l_e) can be calculated using Eq. 1.[23]

$$l_e = \frac{3\mu(2\pi m^* k_B T)^{0.5}}{4e} \quad (1)$$

where k_B, μ, and m^* are Boltzmann constant, carrier mobility, and effective mass, respectively. The effective mass applied in Eq. 1 was calculated by using the experimental Seebeck value and carrier concentration.[24] The so calculated mean free path is between 3 nm and 4 nm depending on the composite, i.e. much lower than the average size of SiC nanoparticles (~50 nm). Because of this significant size difference, charge carriers spend more time within the nanoparticles and go through various scattering mechanisms in addition to phonon scattering leading to the observed reduction in mobility.[25]

The absolute values of the Seebeck coefficient increase with increasing temperature in all cases presented here (Fig. 4). The negative Seebeck value of all composites reflects the fact that electrons are the dominant charge carriers consistent with the Hall effect data. Introducing SiC nanoparticles appears to slightly enhance the Seebeck value especially at higher temperature (above 600 K), reaching the maximum value of -215 μV K^{-1}at 773 K for the sample containing 1 wt.% SiC. This value is compared to the pristine sample with $S = -202$ μV K^{-1}, and corresponds to an increase of 6%, thus barely significant. The slight enhancement of the Seebeck coefficient for the composites might partially stem from the filtering effect caused by the nanoparticle–matrix interface.[26] The 0.5 wt.% SiC composite also shows a higher $S = -212$ μV K^{-1} at 773 K than the MWCNT and Si nanoparticle composites (Table I), which could be a consequence of its lower carrier concentration.

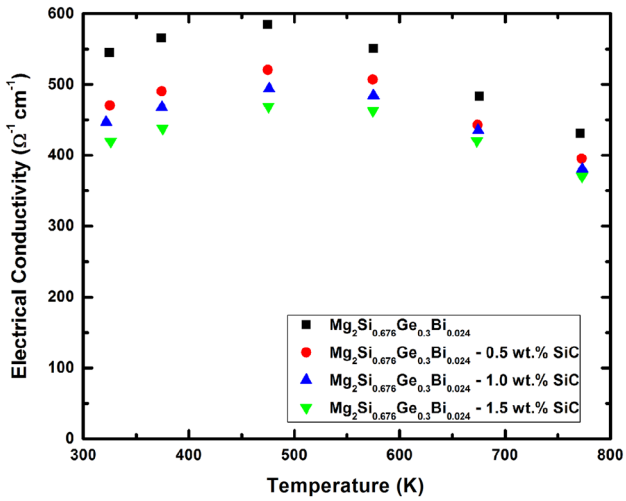

Fig. 2. Electrical conductivity of the $Mg_2Si_{0.676}Ge_{0.3}Bi_{0.024}$/SiC nanocomposites.

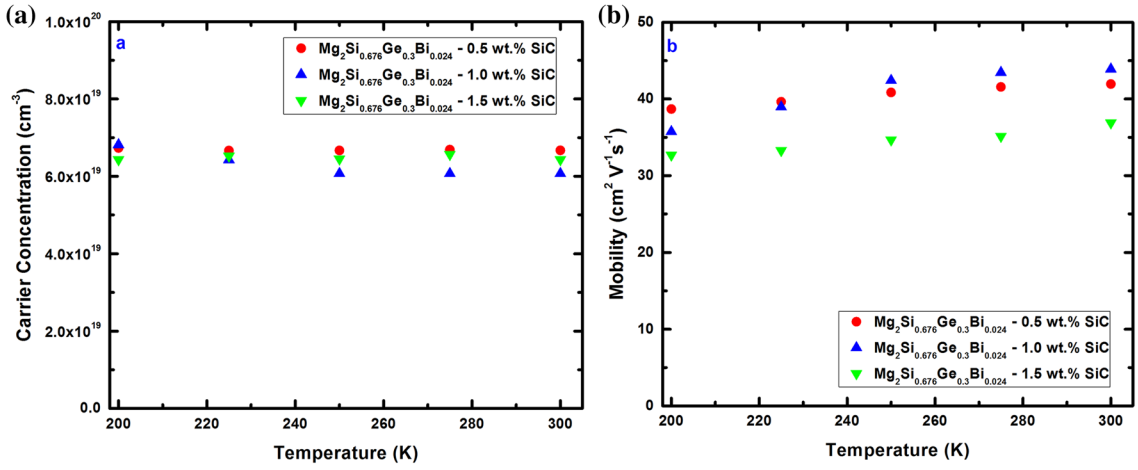

Fig. 3. (a) Low temperature carrier concentration; (b) low temperature Hall mobility of the $Mg_2Si_{0.676}Ge_{0.3}Bi_{0.024}$/SiC nanocomposites.

Table I. Thermoelectric properties of $Mg_2Si_{0.676}Ge_{0.3}Bi_{0.024}$/0.5% SiC at 773 K in comparison to other nanocomposites

	$Mg_2Si_{0.676}Ge_{0.3}Bi_{0.024}$/0.5% SiC	$Mg_2Si_{0.877}Ge_{0.1}Bi_{0.023}$/0.5% MWCNT[20]	Mg_2Si/2.5 mol.% $Si_{1\%Bi}$[14]
$\sigma/(\Omega^{-1}\ cm^{-1})$	396 ± 12	470	658
$S/(\mu V\ K^{-1})$	–212 ± 6	–200	–204
$\kappa/(W\ m^{-1}\ K^{-1})$	1.82 ± 0.09	2.15	3.1
$L/(10^{-8}\ V^2K^{-2})$	1.66	1.62	2.2
$\kappa_L/(W\ m^{-1}\ K^{-1})$	1.31	1.56	2.0
$\mu/(cm^2\ V^{-1}s^{-1})$ [300 K]	42 ± 1	39.5	13
$n/(10^{19}\ cm^{-3})$ [300 K]	6.7 ± 0.1	7.6	11.7
zT [773 K]	0.75 ± 0.08	0.67	0.67

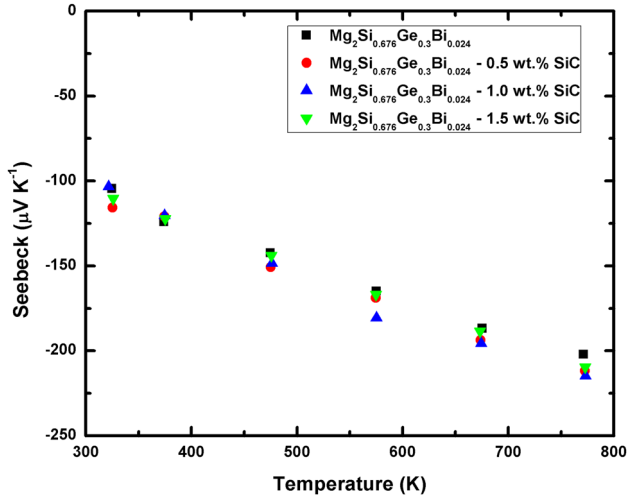

Fig. 4. Seebeck coefficient of the $Mg_2Si_{0.676}Ge_{0.3}Bi_{0.024}$/SiC nanocomposites.

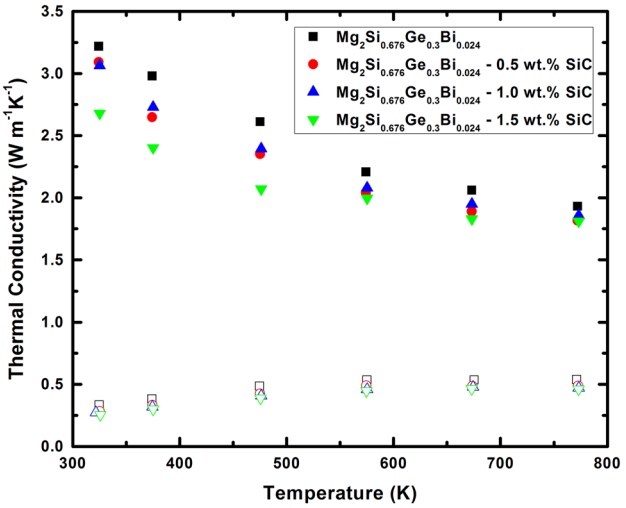

Fig. 5. Total thermal conductivity (solid symbols) and its electronic contribution (open symbols) of the $Mg_2Si_{0.676}Ge_{0.3}Bi_{0.024}$/SiC nanocomposites.

The thermal conductivity of all samples decreases with increasing temperature (Fig. 5a), due to the dominance of Umklapp scattering. All the samples containing SiC have lower thermal conductivity and diffusivity (Figure S4) than the pristine sample, which could be due to the presence of various Bi rich regions (in addition to the increased number of scattering interfaces) at the grain boundaries that can scatter different ranges of phonons. This effect was observed before in skutterudite samples containing Ag nanoparticles.[27] The sample containing 1.5 wt.% SiC displays the lowest room temperature thermal conductivity of 2.68 $W\ m^{-1}\ K^{-1}$, which is approximately 20% lower than that of the pristine sample. The 0.5 wt.% SiC composite reaches the minimum value of 1.82 $W\ m^{-1}\ K^{-1}$, drastically lower than the 0.5 wt.% MWCNT composite (Table - I), which may be in part due to the different Si/Ge ratio.

The electronic thermal conductivity, κ_e, of all samples (Fig. 5) was extracted from the electrical conductivity, σ, by using the Wiedemann–Franz relation, $\kappa_e = L\sigma T$. To obtain the temperature dependent Lorenz numbers L (Figure S5), needed to calculate κ_e, the approximation introduced and validated by Kim et al.[28] was applied, as expressed in Eq. 2:

$$L = \left(1.5 + e^{-\frac{|S|}{\left(116\frac{\mu V}{K}\right)}}\right)10^{-8}V^2K^{-2} \qquad (2)$$

All the nanocomposites show lower κ_{ph} than the pristine sample (Figure S6), with the minimum value of 1.31 $W\ m^{-1}\ K^{-1}$ at 773 K belonging to the sample with 0.5 wt.% SiC. This value is lower than the ones obtained for the MWCNT and Si nanoparticle composites as listed in Table I, possibly related to the above-mentioned differences in the microstructure. The κ_e of all samples increases at first with increasing temperature and then saturates at around 0.5 $W\ m^{-1}\ K^{-1}$ above 600 K. It can

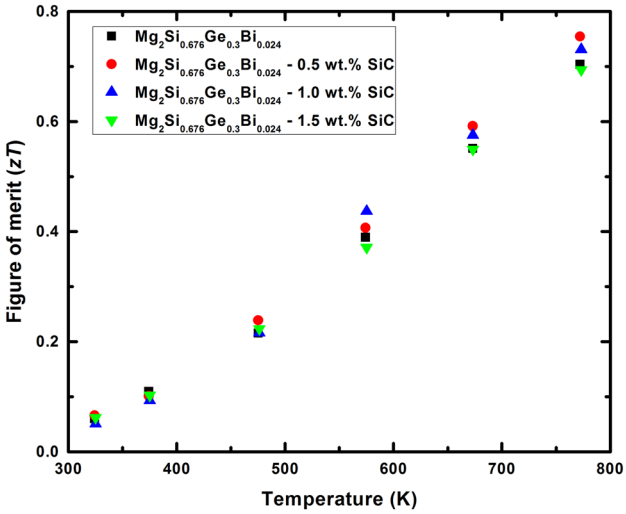

Fig. 6. Figure of merit of the $Mg_2Si_{0.676}Ge_{0.3}Bi_{0.024}$/SiC nanocomposites.

be concluded that the reduction in total thermal conductivity mainly originates from lower κ_{ph}, due to the similarity of κ_e for all samples. The high temperature κ values all converge to a value of approximately 1.85 W m^{-1} K^{-1} at 773 K, which could be due to increasing charge carrier phonon interactions at high temperatures that compensate for the scattering effect coming from nanoparticles.

Figure 6 shows the thermoelectric figure of merit zT as a function of temperature in the range of 300–800 K. The figure of merit of all samples increases with increasing temperature, with the highest values reached by the 0.5 wt.% SiC sample. This culminates in zT = 0.75 at 773 K, which is higher than the zT values achieved for the $Mg_2Si_{1-x}Ge_x$ and Mg_2Si nanocomposites (Table I). To check for homogeneity and reproducibility, a second piece was cut from a different part of the same 0.5 wt.% SiC pellet was used for a new measurement, and the reproduced power factor (Figure S7) is within the estimated experimental error.

CONCLUSIONS

Introducing SiC into $Mg_2Si_{0.676}Ge_{0.3}Bi_{0.024}$ matrix not only affected acoustic phonon scattering, which led to the lowest thermal conductivity of 1.81 W m^{-1} K^{-1} at 773 K, but also impaired the mobility of the charge carriers. The fact that the nanoparticles are about 12 times larger size than the electron mean free path (3–4 nm), leads to a decreased relaxation time of charge carriers, which then resulted in the lowest electrical conductivity of 370 Ω^{-1} cm^{-1} at 773 K for the sample containing the highest wt.% of SiC. Because of the nominally equivalent Bi doping level of all composites in addition to the small SiC concentrations, all the composites exhibited similar carrier concentration of approximately 6.5×10^{19} cm^{-3} between 200 K and 300 K. The EDX line scan of the grain boundary revealed a Bi rich character at the grain boundaries of the $Mg_2Si_{0.676}Ge_{0.3}Bi_{0.024}$/SiC composite, which could be a helpful insight for a grain boundary engineering approach. All in all, the sample with 0.5 wt.% SiC reached a maximum zT of 0.75 at 773 K, which is about 10% higher than that of the SiC-free sample—a change likely in the range of experimental error. In the future, the effect of adding different sizes of SiC nanoparticles on the microstructure and thermoelectric properties of superior $Mg_2Si_{1-x}Sn_x$ based materials can be studied.

ACKNOWLEDGEMENTS

The authors would like to thank AUTO21 (Network Centres of Excellence), General Motors, and the Dana Corporation for financial support of this work. The EDX work in the STEM was carried out at the Canadian Centre for Electron Microscopy, a national facility supported by the Canada Foundation for Innovation, the Natural Sciences and Engineering Research Council of Canada (NSERC), and McMaster University.

ELECTRONIC SUPPLEMENTARY MATERIAL

The online version of this article (doi: 10.1007/s11664-016-4892-8) contains supplementary material, which is available to authorized users.

REFERENCES

1. R.R. Furlong and E.J. Wahlquist, *Nucl. News* 42, 26 (1999).
2. J. Yang and T. Caillat, *MRS Bull.* 31, 224 (2006).
3. M. Matsumoto, M. Mori, T. Haraguchi, M. Ohtani, T. Kubo, K. Matsumoto, and H. Matsuda, *SAE Int. J. Engines* 8, 1815 (2015).
4. M.V. Vedernikov and E.K. Iordanishvili, in *Seventeenth International Conference on Thermoelectronics. Proceedings of ICT98 IEEE* (1998), pp. 37–42.
5. S. LeBlanc, S.K. Yee, M.L. Scullin, C. Dames, and K.E. Goodson, *Renew. Sustain. Energy Rev.* 32, 313 (2014).
6. N. Satyala and D. Vashaee, *J. Electron. Mater.* 41, 1785 (2012).
7. M. Akasaka, T. Iida, A. Matsumoto, K. Yamanaka, Y. Takanashi, T. Imai, and N. Hamada, *J. Appl. Phys.* 104, 013703 (2008).
8. N. Farahi, S. Prabhudev, G. Botton, J. Zhao, J.S. Tse, Z. Liu, J.R. Salvador, and H. Kleinke, *J. Alloys Compd.* 644, 249 (2015).
9. S.K. Bux, M.T. Yeung, E.S. Toberer, G.J. Snyder, R.B. Kaner, and J.-P. Fleurial, *J. Mater. Chem.* 21, 12259 (2011).
10. S.V. Faleev and F. Léonard, *Phys. Rev. B* 77, 214304 (2008).
11. M. Zebarjadi, K. Esfarjani, A. Shakouri, J.-H. Bahk, Z. Bian, G. Zeng, J. Bowers, H. Lu, J. Zide, and A. Gossard, *Appl. Phys. Lett.* 94, 202105 (2009).
12. M.S. Dresselhaus, G. Chen, M.Y. Tang, R.G. Yang, H. Lee, D.Z. Wang, Z.F. Ren, J.-P. Fleurial, and P. Gogna, *Adv. Mater.* 19, 1043 (2007).

13. D. Cederkrantz, N. Farahi, K.A. Borup, B.B. Iversen, M. Nygren, and A.E.C. Palmqvist, *J. Appl. Phys.* 111, 023701 (2012).
14. T. Yi, S. Chen, S. Li, H. Yang, S. Bux, Z. Bian, N.A. Katcho, A. Shakouri, N. Mingo, J.-P. Fleurial, N.D. Browning, and S.M. Kauzlarich, *J. Mater. Chem.* 22, 24805 (2012).
15. S. Fiameni, S. Battiston, S. Boldrini, A. Famengo, F. Agresti, S. Barison, and M. Fabrizio, *J. Solid State Chem.* 193, 142 (2012).
16. V.K. Zaitsev, M.I. Fedorov, E.A. Gurieva, I.S. Eremin, P.P. Konstantinov, A.Y. Samunin, and M.V. Vedernikov, *Phys. Rev. B* 74, 045207 (2006).
17. G.A. Slack, *J. Appl. Phys.* 35, 3460 (1964).
18. D.-W. Liu, J.-F. Li, C. Chen, and B.-P. Zhang, *J. Electron. Mater.* 40, 992 (2010).
19. J.-F. Li and J. Liu, *Phys. Status Solidi* 203, 3768 (2006).
20. N. Farahi, S. Prabhudev, M. Bugnet, G. Botton, J. Zhao, J.S. Tse, J.R. Salvador, and H. Kleinke, *RSC Adv.* 5, 65328 (2015).
21. T. Ikeda, L. Haviez, Y. Li, and G.J. Snyder, *Small* 8, 2350 (2012).
22. N. Nandihalli, S. Gorsse, and H. Kleinke, *J. Solid State Chem.* 226, 164 (2015).
23. Y. Zheng, Q. Zhang, X. Su, H. Xie, S. Shu, T. Chen, G. Tan, Y. Yan, X. Tang, C. Uher, and G.J. Snyder, *Adv. Energy Mater.* 5, 1401391 (2015).
24. G.J. Snyder and E.S. Toberer, *Nat. Mater.* 7, 105 (2008).
25. M. Zebarjadi, K. Esfarjani, M.S. Dresselhaus, Z.F. Ren, and G. Chen, *Energy Environ. Sci.* 5, 5147 (2012).
26. D.L. Medlin and G.J. Snyder, *Curr. Opin. Colloid Interface Sci.* 14, 226 (2009).
27. X. Zhou, G. Wang, L. Zhang, H. Chi, X. Su, J. Sakamoto, and C. Uher, *J. Mater. Chem.* 22, 2958 (2012).
28. H.-S. Kim, Z.M. Gibbs, Y. Tang, H. Wang, and G.J. Snyder, *APL Mater.* 3, 041506 (2015).